von Karman Institute for Fluid Dynamics

Lecture Series 2025-01

MEASUREMENT, MODELLING AND SIMULATIONS TECHNIQUES FOR NOVEL AIRCRAFT ARCHITECTURES

November 4-6, 2024

REVIEW OF AEROACOUSTIC ANALOGIES AND APPLICATIONS TO URBAN AIR MOBILITY

C. Schram[1] & M. Roger[2]
[1]von Karman Institute for Fluid Dynamics, Belgium
[2]Ecole Centrale de Lyon, France

1 Acoustic Analogies

The sound produced by an unsteady flow is fluid oscillatory motion able to propagate away from the flow in the surrounding medium. As such, it could be in principle considered as a part of the flow, the latter being now including also the surrounding propagation medium. This view makes aeroacoustic problems hardly solved by direct numerical simulations of Navier-Stokes equations in situations of engineering interest. Indeed, the simulation framework should be compressible and unsteady by definition, and the required mesh size would be prohibitive. The alternative provided by the Lattice-Boltzmann method (LBM) also remains often very costly. Acoustic analogies allow to formulate the problem in a much more affordable way, by separating the descriptions of the flow and of the acoustic field, in other words separating the predictions of the sources and of their sound radiation. The argument is that sound radiation is a by-product of the flow, carrying a negligible part of its total energy, in other words an energy dissipation process. A numerical simulation of the flow only, ignoring the acoustic dissipation, is much more accessible; once it is made available, the analogies provide a dedicated post-processing. Of course, this interpretation is only valid as long as no back-reaction of the sound on the flow takes place. In engineering context, the analogies also provide a background for analytical modeling, leading to low-cost and fast-running prediction schemes.

The main idea of an analogy is to select a field variable, potentially concentrating the acoustic information, and to restate the general equations of gas dynamics in the form of a standard wave equation for this variable. The procedure interprets as equivalent sources all terms produced by the reformulation which depart from the classical wave operator. The interest is that a formal solution is obtained by a straightforward application Green's formalism to solve the wave equation. But the result is implicit, in the sense that the source terms, in general, contain the selected field variable. Approximations are needed to force the result to become explicit, by simplifications in the source terms. This imposes to ignore mechanisms, expected to be of secondary importance. Therefore, the analogy is useful if the dominant physics is preserved in the approximations. Now the degree of required approximation to get benefit from the linear acoustics framework depends on the available computational resources for the description of the flow itself, ignoring its acoustic dissipation.

1.1 Conservation equations in fluid dynamics for low Mach number flows

In this Section we remind the basic equations describing fluid motion in absence of heat transfer nor variation of the internal energy of the system. The Mach number will be further assumed small enough to assume incompressible behavior. The focus will therefore be placed on the mass conservation and momentum equations, decoupled from the energy equation, to support the derivation of Lighthill's analogy.

The rate of change of the density observed while moving with the fluid velocity is equal to minus the dilatation rate (Batchelor, 1967):

$$\frac{1}{\rho}\frac{\mathrm{D}\rho}{\mathrm{D}t} = -\nabla \cdot \mathbf{v} \tag{1}$$

where the Lagrangian time derivative $\mathrm{D}\rho/\mathrm{D}t$ is related to the Eulerian time derivative $\partial\rho/\partial t$ by:

$$\frac{\mathrm{D}\rho}{\mathrm{D}t} = \frac{\partial\rho}{\partial t} + (\mathbf{v}\cdot\nabla)\rho\,. \tag{2}$$

Substitution of definition (2) into (1) yields the mass conservation law applied to a fixed infinitesimal volume element:

$$\frac{\partial\rho}{\partial t} + \nabla\cdot(\rho\mathbf{v}) = 0\,. \tag{3}$$

For incompressible flows, we have a divergence free velocity field:

$$\nabla\cdot\mathbf{v} = 0\,. \tag{4}$$

Using Einstein's summation convention we can write (3) for cartesian coordinates $\mathbf{x} = (x_1, x_2, x_3)$ as:

$$\frac{\partial\rho}{\partial t} + \frac{\partial\rho v_i}{\partial x_i} = 0\,. \tag{5}$$

The repetition of an index indicates a summation:

$$\frac{\partial\rho v_i}{\partial x_i} = \frac{\partial\rho v_1}{\partial x_1} + \frac{\partial\rho v_2}{\partial x_2} + \frac{\partial\rho v_3}{\partial x_3}\,. \tag{6}$$

Applying the second law of Newton to a fluid particle, we obtain

$$\rho\,\frac{\mathrm{D}\mathbf{v}}{\mathrm{D}t} = -\nabla\mathbf{\Pi} + \mathbf{f} \tag{7}$$

where $\mathbf{f}$ is the density of the force field acting on the bulk of the fluid, while $-\nabla\mathbf{\Pi}$ corresponds to the forces acting on the fluid surface expressed in terms of a stress tensor $\mathbf{\Pi}$. Using the mass-conservation law (3) we obtain the momentum equation in conservative form:

$$\frac{\partial\rho v_i}{\partial t} + \frac{\partial\rho v_i v_j}{\partial x_j} = -\frac{\partial\Pi_{ij}}{\partial x_j} + f_i \tag{8}$$

where the isotropic part of the tensor Π_{ij} corresponds to the effect of the hydrostatic pressure p, and the deviatoric part σ_{ij} accounts for viscous stresses:

$$\Pi_{ij} = p\,\delta_{ij} - \sigma_{ij}\,. \tag{9}$$

The tensor σ_{ij} is symmetric when the molecular structure of the fluid is statistically isotropic (which is the case for all gases and for simple liquids). Since the hydrostatic pressure accounts for all mean normal stresses, we have:

$$\sigma_{ij} = -2\mu\left(e_{ij} - \frac{1}{3}\frac{\partial v_k}{\partial x_k}\,\delta_{ij}\right) \tag{10}$$

where μ is the dynamic viscosity of the fluid, and

$$e_{ij} = \frac{1}{2}\left(\frac{\partial v_i}{\partial x_j} + \frac{\partial v_j}{\partial x_i}\right)\,. \tag{11}$$

Substituting (10) into (7), we find the Navier-Stokes equation of motion:

$$\rho\,\frac{\mathrm{D}v_i}{\mathrm{D}t} = -\frac{\partial p}{\partial x_i} + \frac{\partial}{\partial x_i}\left[2\mu\left(e_{ij} - \frac{1}{3}\frac{\partial v_k}{\partial x_k}\,\delta_{ij}\right)\right] + f_i\,. \tag{12}$$

If the viscosity μ is uniform over the fluid, we find (in vectorial notation):

$$\rho\,\frac{\mathrm{D}\mathbf{v}}{\mathrm{D}t} = -\nabla p + \mu\,\nabla^2\mathbf{v} + \mathbf{f}\,. \tag{13}$$

1.2 Linearization of the equations of fluid mechanics

The equations of continuity (3) and momentum (7) can be rewritten in a general way:

$$\frac{\partial \rho}{\partial t} + \nabla \cdot (\rho \mathbf{v}) = Q_{\mathrm{m}} \tag{14}$$

and

$$\rho \frac{\mathrm{D}\mathbf{v}}{\mathrm{D}t} = -\nabla p + \nabla \cdot \boldsymbol{\sigma} + \mathbf{f} \tag{15}$$

where the source of mass Q_m has been introduced for convenience. In a general non-relativistic context, mass would not be created in a closed control volume with impervious boundary. But if a part of the control volume boundary is permeable to flow, Q_m represents the amount of mass that is injected within the control volume. It will also be shown below that fluctuations of entropy within a closed control volume behave acoustically as an unsteady volumetric flow rate. Note also that in the above expressions, Q_m represents an iso-kinetic injection of mass, which can be quite difficult to achieve in practice.

Linearization of these equations is performed by decomposing the various quantities into mean values and perturbations:

$$\rho(\mathbf{x}, t) = \rho_0 + \rho'(\mathbf{x}, t) \tag{16}$$
$$p(\mathbf{x}, t) = p_0 + p'(\mathbf{x}, t) \tag{17}$$
$$\mathbf{v}(\mathbf{x}, t) = \mathbf{v}_0 + \mathbf{v}'(\mathbf{x}, t) = \mathbf{v}'(\mathbf{x}, t) \tag{18}$$

where the values subscripted 0 are both constant in time and uniform in space. It is further assumed that the mean velocity field is null. Substituting the decomposition (18) into the conservation equations (14) and (15), and neglecting second order terms, we find the linearized continuity and momentum equations:

$$\frac{\partial \rho'}{\partial t} + \rho_0 \nabla \cdot \mathbf{v}' = Q_{\mathrm{m}} \tag{19}$$

and

$$\rho_0 \frac{\partial \mathbf{v}'}{\partial t} = -\nabla p' + \nabla \cdot \boldsymbol{\sigma}' + \mathbf{f}\,. \tag{20}$$

The acoustic velocity perturbation $\mathbf{v}'$ is eliminated by taking the time derivative of Eq. (19), from which we subtract the divergence of Eq. (20), giving:

$$\frac{\partial^2 \rho'}{\partial t^2} - \nabla^2 p' = -\nabla \cdot \mathbf{f} - \nabla \cdot (\nabla \cdot \boldsymbol{\sigma}') + \frac{\partial Q_{\mathrm{m}}}{\partial t}\,. \tag{21}$$

In order to obtain a linear wave propagation from the equation above, a linearized constitutive equation is formed from the equation of state

$$p = p(\rho, s)\,, \tag{22}$$

where s is the entropy, by applying the chain rule of differentiation:

$$p' = \left(\frac{\partial p}{\partial \rho}\right)_s \rho' + \left(\frac{\partial p}{\partial s}\right)_\rho s'\,. \tag{23}$$

The first term of this linearized constitutive equation defines the square of the isentropic speed of sound:

$$c_0^2 \equiv \left(\frac{\partial p}{\partial \rho}\right)_s \tag{24}$$

where the subscript 0 indicates that we will now assume a homogeneous propagation medium, with a constant and uniform speed of sound.

Substitution of (23) into (21) gives a wave propagation equation for the acoustic pressure perturbation, assuming a uniform and quiescent medium:

$$\frac{1}{c_0^2}\frac{\partial^2 p'}{\partial t^2} - \nabla^2 p' = -\nabla \cdot \mathbf{f} - \nabla \cdot (\nabla \cdot \boldsymbol{\sigma}') + \frac{1}{c_0^2}\left(\frac{\partial p}{\partial s}\right)_\rho \frac{\partial^2 s'}{\partial t^2} + \frac{\partial Q_\mathrm{m}}{\partial t} \tag{25}$$

where the LHS is the D'Alembertian operator $\Box$ applied to the the acoustic pressure perturbation, and the terms on the RHS are regarded as sources of sound. The first one represents the effect of a non-uniform body force field. The second term is related to fluctuating viscous stresses. Comparing the third and fourth terms shows that the acoustic effect of entropy fluctuations can be expressed as an equivalent unsteady injection of mass.

If all the terms on the RHS of Eq. (25) vanish, we obtain the homogeneous wave equation

$$\frac{1}{c_0^2}\frac{\partial^2 p'}{\partial t^2} - \nabla^2 p' = 0 \tag{26}$$

which solution is entirely determined by initial and boundary conditions (e.g. a non-zero normal velocity of the surface bounding the fluid domain). A wave propagation equation can also be formed for the acoustic density perturbation, using the linearized constitutive equation (24):

$$\frac{\partial^2 \rho'}{\partial t^2} - c_0^2 \nabla^2 \rho' = 0 \tag{27}$$

In this purely acoustic framework, the equations (26) and (27) are based on the same assumptions, and therefore formally equivalent. The choice of the density as acoustic variable is the best suited when only mechanical effects, not involving heat conduction, are addressed, because the acoustic motion results from combined effects of inertia and compressibility in a fluid. Other variables can be preferred otherwise, for instance in combustion problems.

1.3 Acoustic multipoles

An important property of the wave propagation equation is the non-unicity of the distribution of sources that can generate a given acoustic far-field. There exists in fact an infinity of different point source arrangements giving rise to the same acoustic far-field. These point sources are categorized as multipoles of increasing orders.

Monopole: this is the most basic point source, symbolically represented by the pulsating sphere depicted in the previous section. The radiation pattern is omnidirectional. Exampled in daily life are the unsteady flow rate at the outlet of an automotive muffler, the modulation of the air flowing out of the lungs through the vibrating focal folds, or the unsteady heat release taking place in a turbulent flame.

Dipole: this corresponds symbolically to a sphere that is now oscillating around its mean position, but with no net change of volume (which would give rise to a monopole), which can be also seen as two adjacent monopoles oscillating with opposite phases. The directivity of the pressure field exhibits a maximum radiation along the oscillation axis of the sphere, and zero pressure on a plane perpendicular to this axis passing through the mean sphere position. Within an aeroacoustic context, dipoles correspond to unsteady force fields.

Quadrupole: can be symbolized as two dipoles in phase oppposition either aligned side by side (lateral quadrupole) or sharing the same axis (longitudinal quadrupole). An example of lateral quadrupolar source is the vibrating bell. In aeroacoustics, quadrupolar radiation is caused by free turbulence.

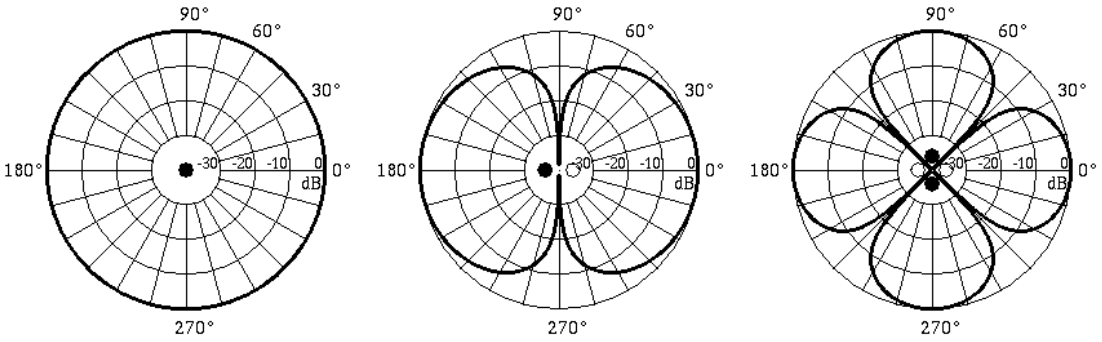


Figure 1: Multipoles: monopole (left), dipole (middle) and lateral quadrupole (right).

The efficiencies of the acoustic multipoles decreases for increasing multipole orders. The acoustic energy radiated by a dipole composed of two monopoles with amplitudes +1 and -1 (i.e. in phase opposition) is much less than the acoustic energy that would be radiated by each constitutive monopole alone. The same reasoning holds for the quadrupole compared to its two constitutive dipoles, a fortiori compared to the four monopoles that compose these two dipoles. It must however be noted that these arguments, are only valid if the building multipoles are separated by a distance that is called *acoustically compact*, i.e. sufficiently smaller than the acoustic wavelength.

1.4 Green's functions

The Green's function formalism is very useful to obtain an integral solution of the wave propagation equation accounting for the effects of the sources, boundary conditions and initial conditions in a fairly straightforward way. The Green's function is defined as the solution of the following inhomogeneous wave equation:

$$\frac{\partial^2 G}{\partial t^2} - c_0^2 \nabla^2 G = \delta(\mathbf{x} - \mathbf{y})\, \delta(t - \tau) \tag{28}$$

where the RHS is the product of two Kronecker delta functions, where $\mathbf{x}$ and t are the listener position and time, and $\mathbf{y}$ is the position of an impulsive source emitting a pulse at the time τ. Boundary conditions must be provided to solve Eq. (28). In free-field

conditions, the appropriate boundary condition is Sommerfeld's (Rienstra and Hirschberg, 2004):

$$\lim_{r\to\infty} r\left(\frac{\partial G}{\partial t} + c_0\,\frac{\partial G}{\partial r}\right) = 0\,. \tag{29}$$

The corresponding solution, noted G_0, is:

$$G_0\left(\mathbf{x},t|\mathbf{y},\tau\right) = \frac{\boldsymbol{\delta}\left(t-\tau-\dfrac{|\mathbf{x}-\mathbf{y}|}{c_0}\right)}{4\pi c_0^2\,|\mathbf{x}-\mathbf{y}|} = \frac{\boldsymbol{\delta}\left(\tau^*-\tau\right)}{4\pi c_0^2\,|\mathbf{x}-\mathbf{y}|} \tag{30}$$

where

$$\tau^* = t - |\mathbf{x}-\mathbf{y}|/c_0 \tag{31}$$

is the *retarded time* at which the source field must be known at the position $\mathbf{y}$ in order to calculate the sound field at the listener position $\mathbf{x}$ at the time t. Furthermore, since a Dirac function is involved, the source field needs to be known at that time only. This important property is valid in the one-dimensional and three-dimensional cases, but not in the two-dimensional case for which the Green's function has a temporal tail requiring to sample the source field for a theoretically infinite number of previous time steps (Dowling and Williams, 1983). For this reason, two-dimensional acoustic propagation problems are often treated in frequency domain.

It can be easily verified that the Green's function above satisfies the so-called *reciprocity* property: $G_0\left(\mathbf{x},t|\mathbf{y},\tau\right) = G_0\left(\mathbf{y},-\tau|\mathbf{x},-t\right)$, i.e. swapping the listener and source positions doesn't change the function as long as the source and listener times are also swapped accordingly. This can be put also as:

$$\frac{\partial G_0}{\partial y_i} = -\frac{\partial G_0}{\partial x_i} \tag{32}$$

$$\frac{\partial G_0}{\partial \tau} = -\frac{\partial G_0}{\partial t} \tag{33}$$

The main purpose of a Green's function consists in finding solutions of the wave propagation equation with a generic source term $q(\mathbf{x},t)$. One proceeds by combining that wave equation multiplied bt G, with the equation (28) itself multiplied by the unknown density perturbation ρ', and integrating the difference of these equations over a control volume V and times from an abitrary time t_0 to the listener time t:

$$\left\{\frac{\partial^2\rho'}{\partial t^2} - c_0^2\,\nabla^2\rho' = q(\mathbf{x},t)\right\} \quad \times G, \iiint_V, \int_{t_0}^{t}$$
$$-\left\{\frac{\partial^2 G}{\partial t^2} - c_0^2\,\nabla^2 G = \boldsymbol{\delta}(\mathbf{x}-\mathbf{y})\,\boldsymbol{\delta}(t-\tau)\right\} \quad \times \rho', \iiint_V, \int_{t_0}^{t}$$

giving:

$$\begin{aligned}\rho'(\mathbf{x},t) = &\int_{t_0}^{t}\iiint_V q(\mathbf{y},\tau)\,G\left(\mathbf{x},t|\mathbf{y},\tau\right)\,\mathrm{d}^3\mathbf{y}\mathrm{d}\tau\\ &+\int_{t_0}^{t}\iiint_V\left(\rho'(\mathbf{y},\tau)\,\frac{\partial^2 G}{\partial\tau^2} - G\,\frac{\partial^2\rho'(\mathbf{y},\tau)}{\partial\tau^2}\right)\,\mathrm{d}^3\mathbf{y}\mathrm{d}\tau\\ &-c_0^2\int_{t_0}^{t}\iiint_V\left(\rho'(\mathbf{y},\tau)\,\frac{\partial^2 G}{\partial y_i^2} - G\,\frac{\partial^2\rho'(\mathbf{y},\tau)}{\partial y_i^2}\right)\,\mathrm{d}^3\mathbf{y}\mathrm{d}\tau\,.\end{aligned} \tag{34}$$

The second and third integrals of Eq. (34) can be integrated by parts with respect to time and space respectively, to yield (with the normal direction defined in Figure 2):

$$\begin{aligned}\rho'(\mathbf{x},t) = &\int_{t_0}^{t} \iiint_V q(\mathbf{y},\tau)\, G\left(\mathbf{x},t|\mathbf{y},\tau\right)\, \mathrm{d}^3\mathbf{y}\mathrm{d}\tau \\ &- \left[\iiint_V \left(\rho'(\mathbf{y},\tau)\,\frac{\partial G}{\partial \tau} - G\,\frac{\partial \rho'(\mathbf{y},\tau)}{\partial \tau}\right)\, \mathrm{d}^3\mathbf{y}\right]_{\tau=t_0}^{\tau=t} \\ &- c_0^2 \int_{t_0}^{t} \iint_{\partial V} \left(\rho'(\mathbf{y},\tau)\,\frac{\partial G}{\partial y_i} - G\,\frac{\partial \rho'(\mathbf{y},\tau)}{\partial y_i}\right)\, n_i\, \mathrm{d}^2\mathbf{y}\mathrm{d}\tau\,. \end{aligned} \tag{35}$$

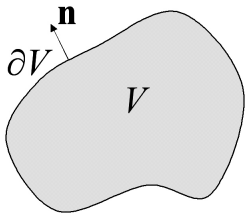


Figure 2: Control volume V, boundary ∂V and outer normal $\mathbf{n}$.

The contribution of the second integral can be brought to zero by virtue of causality and by choosing silent initial conditions. The third integral represents the contribution of the boundaries of the control volume. In absence of solid body in the propagation domain, the only boundary is the one at infinity, where the Green's function and/or source vanishes, giving a null contribution. If a solid body is present, it will from now on be assumed that the control volume boundary coincides with the surface of a solid body. The linearized momentum equation shows that the second term of that integral is related to the wall-normal velocity of the boundary:

$$c_0^2\,\frac{\partial \rho'}{\partial n} = \frac{\partial p'}{\partial n} = -\rho_0\,\frac{\partial v_n'}{\partial t} \tag{36}$$

and is thus equal to zero in case of fixed rigid boundaries, giving:

$$\rho'(\mathbf{x},t) = \int_{t_0}^{t} \iiint_V q(\mathbf{y},\tau)\, G\left(\mathbf{x},t|\mathbf{y},\tau\right)\, \mathrm{d}^3\mathbf{y}\mathrm{d}\tau - c_0^2 \int_{t_0}^{t} \iint_{\partial V} \rho'(\mathbf{y},\tau)\,\frac{\partial G}{\partial n}\,\mathrm{d}^2\mathbf{y}\mathrm{d}\tau \tag{37}$$

where the surface integral represents the scattering of the incident field (first integral) on the domain boundary. It makes Eq. (37) implicit, since the sound field at the listener depends on the acoustic reflections over the surfaces. Solving this equation is in general difficult for arbitrary shapes of the bounding surface, and requires dedicated numerical techniques such as Finite Element Method (FEM) or Boundary Element Methods (BEM).

There are however a number of instances in which solutions of Eq. (37) can be relatively easily obtained. It suffices to observe that if, instead of using the free-field Green's function G_0 , one can adopt a so-called tailored Green's function G_t satisfying Eq. (28) *and* the condition $\partial G/\partial n$ over the boundary S, the contribution of the surface integral vanishes, yielding an explicit integral solution for the acoustic density perturbation:

$$\rho'(\mathbf{x},t) = \int_{t_0}^{t} \iiint_V q(\mathbf{y},\tau)\, G_t\left(\mathbf{x},t|\mathbf{y},\tau\right)\, \mathrm{d}^3\mathbf{y}\mathrm{d}\tau\,. \tag{38}$$

The geometrical configurations for which such tailored Green's functions can be found are unfortunately not numerous. If the scattering surface is an infinite plane, the method of images can be applied to find a tailored Green's function. Other examples are straight ducts with canonical cross-shapes (circular, annular, rectangular), for which a solution of Eq. (28) can be obtained by separation of variables (Rienstra and Hirschberg, 2004).

1.5 Lighthill's Analogy

Due to the non-linearity of the governing equations and the importance of different scales it is a difficult task to predict the sound production by fluid flows. As the sound field associated to subsonic flows represents only a very minute fraction of the energy in the flow, the accuracy of numerical simulations must be very high to predict the sound generation and propagation. This is particularly dramatic in free space and at low subsonic speeds.

The fact that the sound field is in some sense a small perturbation of the flow, can however be used to obtain approximate solutions. Aeroacoustical analogies have been developed for this purpose.

An aeroacoustical analogy is a reformulation of the fluid dynamics equations that allows to distinguish the sound generation mechanisms from the sound propagation. The part of the flow in which sound production is expected is called the *source region*. The part of the flow in which the listener is standing defines the *reference flow*. The difference between the actual flow and an extrapolation of the reference flow into the source region is identified as the source of sound. This idea was introduced by Lighthill (1952) who calls this an *analogy*.

In some cases, the distinction between sound production and sound propagation mechanisms can be delicate. These aspects can even become coupled when aero-acoustical or thermo-acoustical resonances occur. One has then to resort on CFD accuracy to capture the coupling phenomenon. This imposes severe accuracy requirements for the compressible numerical simulation that must be used in order to capture the acoustic propagation and feedback on the source mechanism (vortex shedding, flame response...). Fortunately, such resonances involve generally large-scale flow features, which can be reasonably computed by Large Eddy Simulation or Detached Eddy Simulation. The corresponding acoustical wavelengths are often large compared to the typical geometrical dimensions, which leads to moderate numerical dispersion and dissipation over the region where the coupling occurs. In any case, flow-acoustic resonances are not considered in this Section, where it is assumed that the sound emitted by the low Mach number flow doesn't perturb that flow.

1.5.1 A reformulation of the conservation equations

Lighthill's analogy is derived from the exact mass conservation equation (5) and momentum equation (8). We take the time derivative of the mass equation (5) and subtract from this the divergence of the momentum equation (8) to obtain:

$$\frac{\partial^2 \rho}{\partial t^2} = \frac{\partial^2 (\rho v_i v_j - \sigma_{ij})}{\partial x_i \partial x_j} + \frac{\partial^2 p}{\partial x_i^2} - \frac{\partial f_i}{\partial x_i} \,. \tag{39}$$

We can subtract on both sides of this equation a term $c_0^2(\partial^2\rho/\partial x_i^2)$ were c_0 is a velocity. This provides an equation in which the left hand side is the wave propagation operator of

d'Alembert:

$$\frac{\partial^2 \rho}{\partial t^2} - c_0^2 \frac{\partial^2 \rho}{\partial x_i^2} = \frac{\partial^2 (\rho v_i v_j - \sigma_{ij})}{\partial x_i \partial x_j} + \frac{\partial^2 (p - c_0^2 \rho)}{\partial x_i^2} - \frac{\partial f_i}{\partial x_i} \,. \tag{40}$$

In order to proceed, the key idea is to compare this equation with the linearized wave propagation equation (27), which we had obtained under normal audio frequency and amplitude conditions for the acoustical propagation in a uniform and stagnant fluid in the state (ρ_0, p_0). It should be noted that these conditions (ρ_0, p_0) were introduced in Eqs. (18) for the purpose of linearizing the governing equations, but they are used here to define a reference uniform and stagnant propagation medium surrounding the jet flow, where the acoustic waves are by definition propagating at the constant speed c_0. Note that these definitions do not restrict in any way the generality of the equation that will follow, known as Lighthill's analogy (Crighton et al., 1992):

$$\frac{\partial^2 \rho'}{\partial t^2} - c_0^2 \frac{\partial^2 \rho'}{\partial x_i^2} = \frac{\partial^2 T_{ij}}{\partial x_i \partial x_j} - \frac{\partial f_i}{\partial x_i} \tag{41}$$

where T_{ij} is the Lighthill stress tensor defined as:

$$T_{ij} = \rho v_i v_j + (p' - c_0^2 \rho') \, \delta_{ij} - \sigma_{ij} \,. \tag{42}$$

It should be noted that the procedure followed here to form a D'Alembertian on the LHS is the same as the one of Section 1.2, with however a substantial difference: there has been no approximation nor linearization, i.e. all non-linearities of the flow field are still included in the RHS of Eq. (41).

In the acoustical flow around the listener the source term represented by the RHS of (41) vanishes. It is indeed assumed that no external forces f_i are exerted in the reference quiescent flow region. Under normal audio conditions we can use a linear approximation so that we neglect $\rho v_i v_j$ in the acoustical field around the observer. Furthermore, we can neglect friction losses σ_{ij} and heat conduction for distances of propagation comparable to the wavelength. Finally, the contribution $(p' - c_0^2 \rho')$ to Lighthill's stress tensor (42) vanishes owing to the speed of sound in this region.

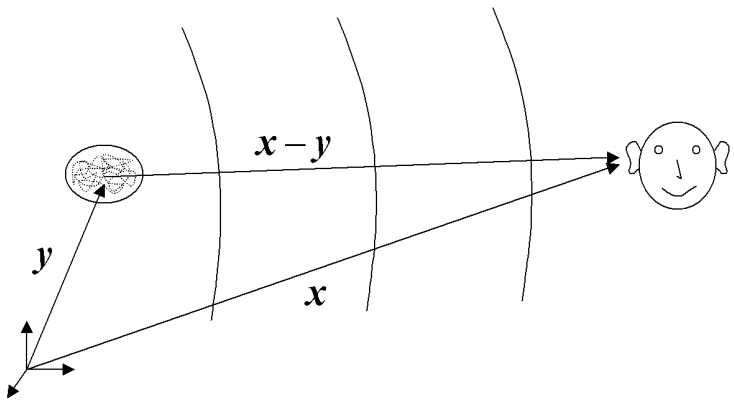


Figure 3: Source and listener in the analogy of Lighthill. While in the source region the density fluctuations are not necessarily small, around the listener we assume an acoustical behavior with $\rho' \ll \rho_0$.

The RHS of (41) expresses therefore the equivalent acoustical sources that correspond to the present choices for the uniform and stagnant reference flow at the listener's position and for the acoustical variable ρ'. Other choices for the reference state and acoustical variable might be more appropriate depending on the application.

We insist on the fact that Equation (41) has been derived from the governing equations making no approximation, simply defining an arbitrary medium representing the region where the listener is located. This expression therefore involves all the unknowns of the original Navier-Stokes equations, and is generally not easier to sove than the latter. It provides however a powerful formalism to introduce quite useful approximations in the description of the source field.

Firstly, the high Reynolds numbers met in typical industrial flows ($\mathrm{O}(10^4 - 10^6)$) allow to neglect the viscous contribution σ_{ij} with respect to the inertial term $\rho v_i v_j$. We can thus safely drop the term σ_{ij} in most practical applications. A second simplification can be made when the flow field in the source region behaves in an isentropic fashion. This assumption is usually fairly resaonable at low Mach numbers and in absence of thermo-diffusive processes. It can obviously not be made to describe combustion noise processes.

1.5.2 Integral solution

We have seen in Section 1.4 how to solve the inhomogeneous wave propagation equation (41) using a Green's function. Using the same arguments about causality and initial silent boundary conditions, we end up with a very similar equation:

$$\rho'(\mathbf{x},t) = \int_{-\infty}^{t} \iiint_V \frac{\partial^2 T_{ij}}{\partial y_i \partial y_j}\, G\, \mathrm{d}^3\mathbf{y}\mathrm{d}\tau - c_0^2 \int_{-\infty}^{t} \iint_{\partial V} \left(\rho' \frac{\partial G}{\partial y_i} - G \frac{\partial \rho'}{\partial y_i}\right) n_i\, \mathrm{d}^2\mathbf{y}\, \mathrm{d}\tau \qquad (43)$$

where the first integral represents the incident sound field due to the aerodynamic sources distributed in the fluid volume V, and the second integral represents the scattering over the boundaries ∂V of this volume and possible vibration of a solid surface bounding the volume. In absence of solid bodies, the only contribution from the boundary is from its portion at infinity such that the contribution of the surface integral vanishes. In presence of solid bodies, the contribution of the scattering part of the integral can also be brought to zero by finding a suitable *tailored* Green's function such as $\partial G/\partial n = 0$ on ∂V, as explained in Section 1.4. The choice of a free field Green's function in presence of solid boundaries corresponds to Curle's analogy, discussed in Section 1.6.

We consider first the case of free field conditions, and the integration volume extends to infinity. The volume source integral of (43) can be integrated two times with respect

to space:

$$\int_{-\infty}^{t} \iiint_V \frac{\partial^2 T_{ij}}{\partial y_i \partial y_j}\, G\, \mathrm{d}^3\mathbf{y}\, \mathrm{d}\tau = \int_{-\infty}^{t} \iint_{\partial V} \frac{\partial T_{ij}}{\partial y_i}\, G\, n_j\, \mathrm{d}^2\mathbf{y}\, \mathrm{d}\tau - \int_{-\infty}^{t} \iint_V \frac{\partial T_{ij}}{\partial y_i}\, \frac{\partial G}{\partial y_j}\, \mathrm{d}^3\mathbf{y}\, \mathrm{d}\tau$$
$$= \int_{-\infty}^{t} \iint_{\partial V} \left(\frac{\partial T_{ij}}{\partial y_i}\, G\, n_j - T_{ij}\, \frac{\partial G}{\partial y_j}\, n_i \right) \mathrm{d}^2\mathbf{y}\, \mathrm{d}\tau$$
$$+ \int_{-\infty}^{t} \iiint_V T_{ij}\, \frac{\partial^2 G}{\partial y_i \partial y_j}\, \mathrm{d}^3\mathbf{y}\, \mathrm{d}\tau\,. \tag{44}$$

where the surface integral vanishes at infinity.

1.5.3 Considerations on numerical robustness

The integration by parts that was performed above proves in practice very useful, for two main reasons. The first reason holds in the uncertainty that is often inherent to the term T_{ij}, which includes inevitably some error whatever the modeling approach. It is therefore preferable to have to derive the perfectly known Green's function. The second reason stands in the effective multipolar character that is attributed to the source field depending on the form under which the free-field Green's function appears in the convolution integral. This argumentation will be come clearer below, but in short the convolution with G_0 indicates a monopolar efficiency, using $\partial G_0/\partial y_i$ yields a dipolar efficiency, and with $\partial^2 G_0/\partial y_i \partial y_j$ we obtain a quadrupolar efficiency. Given a monopole is acoustically much more efficient than a dipole, itself more efficient than a quadrupole, it should be made clear that a formulation which attempts to model a quadrupole as a combination of monopoles or dipoles will suffer from numerical robustness issues, because any net spurious monopole or dipole will radiate with their own efficiency and overwhelm the desired quadrupole.

This is exemplified by a numerical exercise illustrated in Figure 4, where a quadrupole of amplitude $T_{xy} = 1$ (all other components being null) has been treated:

- as a quadrupole indeed, multiplying it with $\partial^2 G_0/\partial y_i \partial y_j$;
- as two opposite dipoles (convoluted by $\partial G_0 \partial y_i$) aligned in the x-direction placed side-by-side at the coordinates $(x, y, z) = (0, \pm 0.015, 0)\,\lambda$;
- as four quadrupoles (convoluted by G_0) placed at the coordinates $(x, y, z) = (\pm 0.015, \pm 0.015, 0)\,\lambda$;

where λ is the acoustic wavelength.

The acoustic pressure modulus is represented in Figure 5 (with identical color scaling) over a sphere with radius about 30λ. The amplitudes given the individual dipoles and monopoles have been adjusted to obtain the same amplitude in the undisturbed case. Only one component of the multipole assemblies has been perturbed by adding 5% to its amplitude. The results show that the same far-field radiation can be obtained by the three methods if no net dipole or monopole is present. The numerical calculation of the

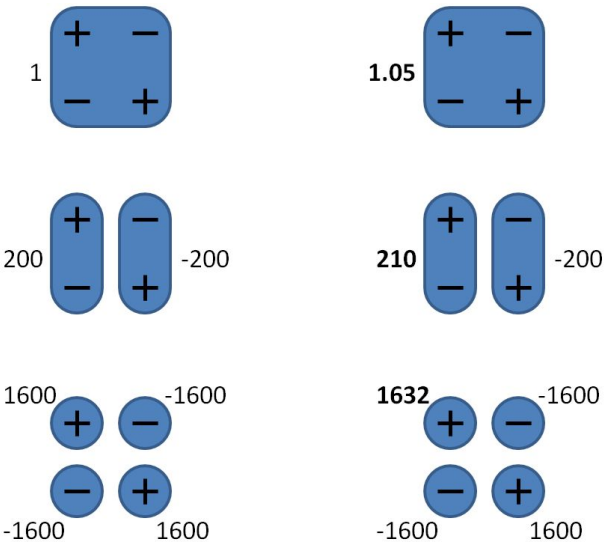
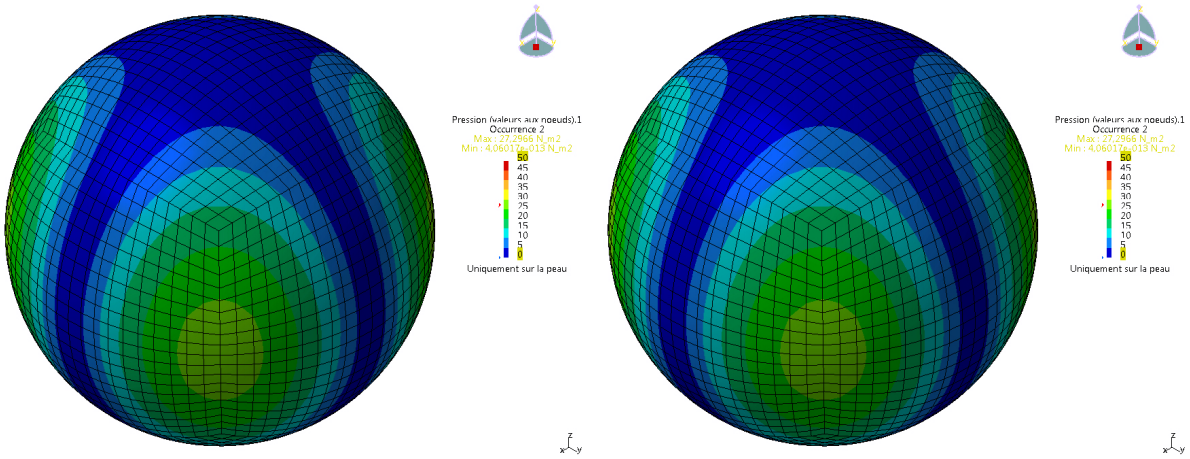
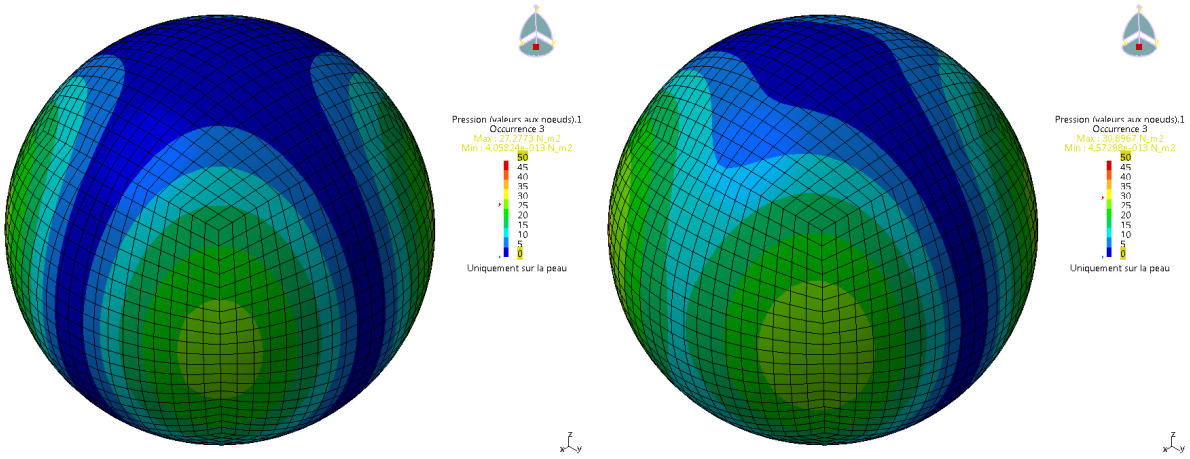


Figure 4: Representation of a lateral quadrupole as a single point quadrupole, two point dipoles or 4 point monopoles (left column), and with 5% perturbation added to one of the constituants (right column). The amplitudes in the undisturbed case are arbitrarily adjusted to give the same net far-field radiation owing to the conventions used in the numerical acoustics solver.

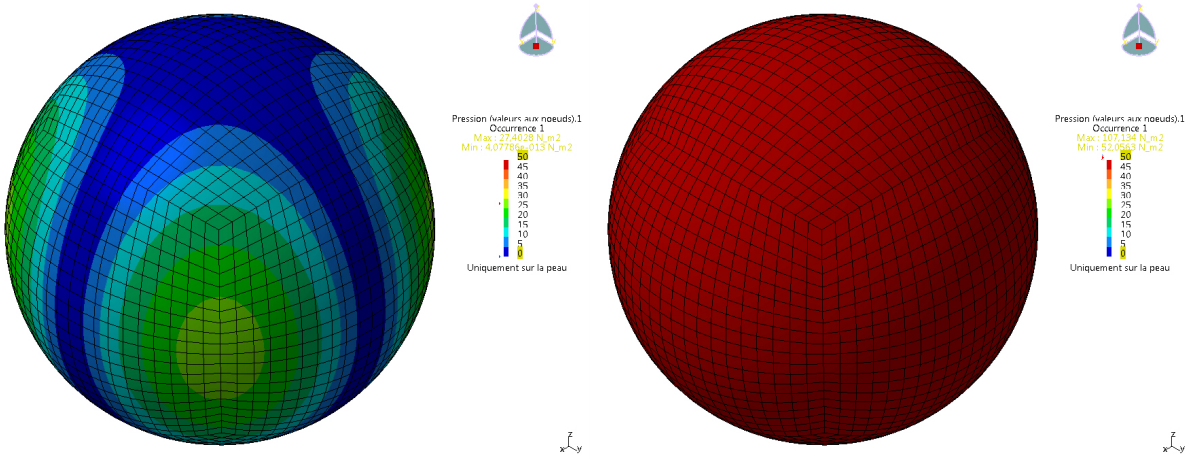
interferences yields the correct directivity pattern and efficiency. However, it is also seen that introducing an error as small as 5% to one of the constitutive dipoles or monopoles alters significantly both directivities and amplitudes of the acoustic field, which are in fact imposed by the small net dipole or monopole component.



5.1: Left: one quadrupole $T_{xy} = 1$; right: one quadrupole $T_{xy} = 1.05$.



5.2: Left: two dipoles with amplitudes $D_{x,1-2} = \pm 200$ (left); right: $D_{x,1} = 210$, $D_{x,2} = 200$.



5.3: Left: four monopoles with amplitudes $M_{x,1-4} = \pm 1600$ (left); right: $M_{x,1} = 1680$, $M_{x,2-4} = 1600$

Figure 5: Acoustic pressure magnitude obtained using alternative representations of the same quadrupole showing the numerical robustness when an error as small as 5% is added to one of the constituants (i.e. 5% spurious monopole or dipole).

1.5.4 Sound power generated by subsonic free jets: the M^8 scaling law

Using the high Reynolds number and isentropic assumptions introduced above, using the symmetry properties (33) of the Green's function, and performing the integration in time we obtain:

$$\rho'(\mathbf{x},t) = \frac{\partial^2}{\partial x_i \partial x_j} \iiint_V \left[\frac{\rho v_i v_j}{4\pi c_0^2 |\mathbf{x}-\mathbf{y}|} \right] \mathrm{d}^3\mathbf{y} \tag{45}$$

where the bracketed terms have to be evaluated at the retarded time $\tau^* = t - |\mathbf{x}-\mathbf{y}|/c_0$. Equation (45) provides an integral solution, however this is not yet an explicit solution, since the density in the source term contains both the hydrodynamic and acoustical density perturbations. We have to introduce a further approximation to obtain an explicit solution, based on the fact that for low Mach isothermal flow in the source region, the relative density fluctuations scale as M^2. We make therefore the approximation $\rho v_i v_j \simeq \rho_0 v_i v_j$ where ρ_0 is the density in the reference propagation region, to find:

$$\rho'(\mathbf{x},t) = \frac{\partial^2}{\partial x_i \partial x_j} \iiint_V \left[\frac{\rho_0 v_i v_j}{4\pi c_0^2 |\mathbf{x}-\mathbf{y}|} \right] \mathrm{d}^3\mathbf{y} \tag{46}$$

Note that the incompressible flow approximation restricts the application of (46) to cases where no acoustic feedback occurs from the propagation region back to the source. In order to apply the analogy to resonant cases, the resonant mechanism must be included in the source description. Practically, this implies that a sufficiently accurate compressible flow calculation must be employed in the aero-acoustic coupled region.

The result (46) permits to derive an order of magnitude of the sound energy produced by turbulent flows (Lighthill, 1954). When the listener is in the far field, the relevant local length scale is the acoustical wavelength. Assuming that the sound production is dominated by the large turbulent structures scaling with the nozzle diameter D, and for which the typical convection velocity scales with U_0, the flow time scale is D/U_0. We can therefore replace each spatial derivative by a multiplication by a factor $U_0/(c_0 D)$. Assuming $U_0/c_0 \ll 1$ appears then to be equivalent to the assumption of a compact flow region (small compared to the acoustical wavelength). The integrand in (46) scales as $\rho_0 U_0^2 D^3/(c_0^2|\mathbf{x}|)$, so that the order of magnitude of the pressure perturbation is

$$p' = c_0^2 \rho' \propto \frac{U_0^2}{c_0^2 D^2} \frac{\rho_0 U_0^2 D^3}{|\mathbf{x}|} = \rho_0 M^2 U_0^2 \frac{D}{|\mathbf{x}|} = \rho_0 c_0^2 M^4 \frac{D}{|\mathbf{x}|} \tag{47}$$

and the sound power radiated scales as

$$W_q = \frac{4\pi |\mathbf{x}|^2 p'^2}{\rho_0 c_0} \propto \rho_0 c_0^3 D^2 M^8 \tag{48}$$

which is Lighthill's famous M^8 law for the quadrupolar sound radiated by low Mach number turbulence in absence of external forces. We emphasize that we found a quadrupolar efficiency because we assume that there are no external forces, which is used as argument to exclude any dipole term. This argument no longer holds in presence of solid surfaces, where a counter-force must be externally applied to balance the flow-induced efforts on the body. This case is discussed hereafter.

1.6 Curle's analogy

Curle extended Lighthill's results for the sound production by unsteady flows interacting with steady surfaces (Curle, 1955). The flow volume boundary ∂V in (43) includes the surface of the solid body, and if we use the free field Green's function G_0 as before, the surface integral will yield the implicit scattering of the volume source over the body surface. Performing the double integration by parts of the volume source in (43), we had previously obtained the following expression:

$$\begin{aligned}\rho'(\mathbf{x},t) = &\int_{-\infty}^{t} \iiint_V T_{ij}\,\frac{\partial^2 G}{\partial y_i \partial y_j}\,\mathrm{d}^3\mathbf{y}\,\mathrm{d}\tau \\ &+ \int_{-\infty}^{t} \iint_{\partial V} \left(\frac{\partial T_{ij}}{\partial y_i}\,G\,n_j - T_{ij}\,\frac{\partial G}{\partial y_j}\,n_i\right)\mathrm{d}^2\mathbf{y}\,\mathrm{d}\tau \\ &- c_0^2 \int_{-\infty}^{t} \iint_{\partial V} \left(\rho'\,\frac{\partial G}{\partial y_i} - G\,\frac{\partial \rho'}{\partial y_i}\right) n_i\,\mathrm{d}^2\mathbf{y}\,\mathrm{d}\tau\,. \end{aligned} \tag{49}$$

Since T_{ij} is a symmetrical tensor, we have $(\partial T_{ij}/\partial y_i)\,n_j = (\partial T_{ij}/\partial y_j)\,n_i$, and using the conservation of momentum (8) in absence of external forces, we find:

$$\begin{aligned}\frac{\partial T_{ij}}{\partial y_j} &= \frac{\partial}{\partial y_j}\,\left(\rho v_i v_j + (p' - c_0^2\,\rho')\,\boldsymbol{\delta}_{ij} - \sigma_{ij}\right) \\ &= -\frac{\partial \rho v_i}{\partial \tau} - c_0^2\,\frac{\partial \rho'}{\partial y_i}\,. \end{aligned} \tag{50}$$

Introducing the expression of the source tensor T_{ij} in (49), we obtain therefore:

$$\begin{aligned}\rho'(\mathbf{x},t) = &\int_{-\infty}^{t} \iiint_V T_{ij}\,\frac{\partial^2 G}{\partial y_i \partial y_j}\,\mathrm{d}^3\mathbf{y}\,\mathrm{d}\tau \\ &+ \int_{-\infty}^{t} \iint_{\partial V} \left\{\left(-\frac{\partial \rho v_i}{\partial \tau} - c_0^2\,\frac{\partial \rho'}{\partial y_i}\right) G - \left(\rho v_i v_j + (p' - c_0^2 \rho')\,\boldsymbol{\delta}_{ij} - \sigma_{ij}\right)\,\frac{\partial G}{\partial y_j}\right\} n_i\,\mathrm{d}^2\mathbf{y}\,\mathrm{d}\tau \\ &- c_0^2 \int_{-\infty}^{t} \iint_{\partial V} \left(\rho'\,\frac{\partial G}{\partial y_i} - G\,\frac{\partial \rho'}{\partial y_i}\right) n_i\,\mathrm{d}^2\mathbf{y}\,\mathrm{d}\tau \end{aligned} \tag{51}$$

and we see that the scattering terms corresponding to the second integral cancel out with the density perturbation terms coming from Lighthill's tensor. We obtain:

$$\begin{aligned}\rho'(\mathbf{x},t) = &\int_{-\infty}^{t} \iiint_V T_{ij}\,\frac{\partial^2 G}{\partial y_i \partial y_j}\,\mathrm{d}^3\mathbf{y}\,\mathrm{d}\tau \\ &- \int_{-\infty}^{t} \iint_{\partial V} \left(\frac{\partial \rho v_i}{\partial \tau}\,G + (\rho v_i v_j + p'\,\boldsymbol{\delta}_{ij} - \sigma_{ij})\,\frac{\partial G}{\partial y_j}\right) n_i\,\mathrm{d}^2\mathbf{y}\,\mathrm{d}\tau \end{aligned} \tag{52}$$

where the first term in the second integral can be integrated by parts (assuming the normal n_i does not vary in time):

$$\int_{-\infty}^{t} \iint_{\partial V} \frac{\partial \rho v_i}{\partial \tau}\, G\, n_i \,\mathrm{d}^2\mathbf{y}\mathrm{d}\tau = \iint_{\partial V} \left[\rho v_i n_i G\right]_{-\infty}^{t} \mathrm{d}^2\mathbf{y} - \int_{-\infty}^{t} \iint_{\partial V} \rho v_i n_i \frac{\partial G}{\partial \tau}\, \mathrm{d}^2\mathbf{y}\mathrm{d}\tau\,. \tag{53}$$

The first integral vanishes either as before by virtue of causality, or simply because the surface or the solid body is here assumed steady and impermeable, thereby cancelling the contribution of the second integral as well. We obtain:

$$\rho'(\mathbf{x},t) = \int_{-\infty}^{t} \iiint_{V} T_{ij} \frac{\partial^2 G}{\partial y_i \partial y_j}\, \mathrm{d}^3\mathbf{y}\, \mathrm{d}\tau - \int_{-\infty}^{t} \iint_{\partial V} \left(p'\,\delta_{ij} - \sigma_{ij}\right) \frac{\partial G}{\partial y_j}\, n_i \,\mathrm{d}^2\mathbf{y}\, \mathrm{d}\tau \tag{54}$$

Note that the above derivations so far are valid irrespectively of the Green's function being free field or tailored. Having a free field Green's function G_0 with space and time reciprocity properties (32-33) and the far field approximation

$$\frac{\partial}{\partial x_i} \simeq -\frac{x_i}{c_0|\mathbf{x}|}\frac{\partial}{\partial t} \tag{55}$$

allows to find:

$$\begin{aligned}\rho'(\mathbf{x},t) = \frac{x_i x_j}{4\pi|\mathbf{x}|^2 c_0^4} \frac{\mathrm{d}^2}{\mathrm{d}t^2} \iiint_{V} \left[\frac{T_{ij}}{|\mathbf{x}-\mathbf{y}|}\right] \mathrm{d}^3\mathbf{y} - \frac{1}{4\pi c_0^2}\frac{\mathrm{d}}{\mathrm{d}t} \iint_{\partial V} \left[\frac{\rho v_i n_i}{|\mathbf{x}-\mathbf{y}|}\right] \mathrm{d}^2\mathbf{y} \\ - \frac{x_i}{4\pi|\mathbf{x}|c_0^3}\frac{\mathrm{d}}{\mathrm{d}t} \iint_{\partial V} \left[\frac{\left(\rho v_i v_j + p'\,\delta_{ij} - \sigma_{ij}\right) n_j}{|\mathbf{x}-\mathbf{y}|}\right] \mathrm{d}^2\mathbf{y}\end{aligned} \tag{56}$$

where bracketed terms are to be evaluated at the retarded time (31). For a steady, non-penetrable surface and assuming a low Mach number, isentropic flow in the source region, the same approximations as above yield:

$$\rho'(\mathbf{x},t) = \frac{x_i x_j}{4\pi|\mathbf{x}|^2 c_0^4} \frac{\mathrm{d}^2}{\mathrm{d}t^2} \iiint_{V} \left[\frac{\rho_0 v_i v_j}{|\mathbf{x}-\mathbf{y}|}\right] \mathrm{d}^3\mathbf{y} - \frac{x_i}{4\pi|\mathbf{x}|c_0^3}\frac{\mathrm{d}}{\mathrm{d}t} \iint_{\partial V} \left[\frac{p' n_i}{|\mathbf{x}-\mathbf{y}|}\right] \mathrm{d}^2\mathbf{y} \tag{57}$$

and the acoustical pressure perturbation is obtained by multiplying (57) by c_0^2.

The first integral of (57) is identical to the one found in the derivation of Lighthill's analogy for free turbulence, and corresponds therefore to the same quadrupolar sound radiation. The second term is a surface integral of the fluctuating pressure on the surface of the solid body, and shows a dipolar directivity. In terms of source efficiency, it can be easily demonstrated that the sound power emitted by a compact steady dipole source scales as $W_d \propto \rho_0 c_0^3 D^2 M^6$. At low Mach numbers, the interaction of turbulence with compact solid surfaces is therefore acoustically M^2 more efficient than the compact lump of turbulence that induces this dipole source on the body. This is related to the decrease of the acoustical efficiency for increasing multipole orders.

Computationally speaking, it is therefore very attractive to neglect the quadrupolar part of the sound field, especially because of the high cost associated with the accurate computation of this second-order, spatially extended turbulent source term and its storage in memory.

Important remark on the use of incompressible flow data with Curle's analogy: while this analogy has proven its ability to predict sound generated by compact bodies, some care must be exercised for non-compact sources (Colonius and Lele, 2004). Acoustic compactness implies that retarded time differences between different parts of the sound emitting surface can be neglected. As a corollary, the compact body does not scatter its own sound, and an incompressible flow model suffices to calculate the dipolar surface integral of (54). But when the unsteady flow produces sound at wavelengths comparable to, or smaller than the body dimensions, scattering effects cannot be neglected anymore, and should be included in the dipolar source term.

In mathematical terms, we had in (43) an original volume integral of the term $\partial^2 T_{ij}/\partial y_i \partial y_j$ to be scattered over the boundaries ∂V of the fluid domain. After integration by parts, we are left in (54) with a modified quadrupolar source term involving T_{ij}, and a dipolar surface integral of both the wall pressure fluctuations p' induced by the corresponding lump of turbulence, *and* the acoustical pressure field of this source. Powell (1960) considers the dipolar integral in (54) as a reflection of the quadrupole of (43).

The derivation of (54) implicitly assumes that compressibility effects are accounted for in the flow region, including acoustic perturbations. The use of an incompressible flow solution does not thus seem appropriate, unless the turbulence/body interaction occurs over a region that is effectively compact enough to yield minor scattering effects. This is for example the case for the aeolien tone or non-resonating short cavity flows, for which the typical Strouhal numbers make the interaction region very compact indeed. The trouble comes when Curle's analogy (54) is used to predict the sound produced by turbulent confined flow interacting with extended geometries (e.g. HVAC systems) extending over several acoustical wavelengths (Pérot et al., 2004) or for high-frequency trailing edge noise (Wang and Moin, 2000).

1.7 Ffwowcs Williams & Hawkings' Formulation

Lighthill's analogy was developed to address sound generation by localized turbulent mixing in unbounded surrounding medium. When analyzing the noise from rotating blades, and more generally when solid surfaces bounding the propagation-and-flow domain must be included, the formulation must be revised. The first logical approach would be to still solve Lighthill's equation, but with a Green's function tailored to the geometry of the solid surfaces, instead of the free-field Green's function. For practical reasons, and for the sake of clear physical insight, a better approach is to reformulate the analogy, by replacing the boundary conditions on the surfaces by additional equivalent sources, in order to recover the homogeneous framework of the unbounded space. This was done by Williams and Hawkings (1969), resorting to generalized functions.

The basic concept is the following: the equations of fluid mechanics are of course only applicable in the domain occupied by the fluid, but we can formulate equations valid everywhere by introducing the generalized functions δ (*delta* function) and H (*Heaviside* function) taking a function F as argument. The essential property of F is to be equal to zero on the surface of the bodies, negative inside the solid bodies and positive in the fluid region (Figure 6). As the iso-surface $F = 0$ is a material surface of the fluid, we have:

$$\frac{\mathrm{D}F}{\mathrm{D}t} = \frac{\partial F}{\partial t} + \mathbf{v} \cdot \nabla F = 0 \tag{58}$$

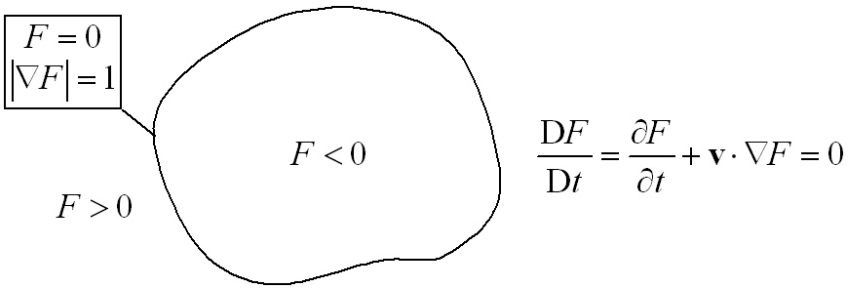


Figure 6: Definition of the function F.

and the properties of the Heaviside function are such that:

$$\begin{aligned} H(F) &= 0 \qquad \text{inside the solid bodies} \\ &= 1 \qquad \text{in the fluid region} \\ \nabla(H(F)) &= \delta(F)\,\nabla F \\ \frac{\partial}{\partial t}(H(F)) &= \delta(F)\,\frac{\partial F}{\partial t} \end{aligned}$$

Impermeable vs. permeable formulations: we have here decided to have the control surface located at the boundary of the solid body, but it could as well be located anywhere inside the fluid. The latter choice leads to the so-called permeable formulation, which shows some numerical advantages in some specific instances, e.g. for transonic and supersonic Mach numbers, when the quadrupolar noise emissions, for example due to shocks, cannot be ignored. The reader is referred to Ianniello (2007) for more thorough dicussion of such cases. The applications considered in this course being limited to the subsonic regime, only the solid – or impermeable – version of the FW-H analogy will be presented.

The equations of continuity and momentum can be rewritten as:

$$\frac{\partial(\rho' H)}{\partial t} + \frac{\partial(\rho v_i H)}{\partial x_i} = \rho_0\,(\mathbf{v}\cdot\nabla F)\,\delta(F) = \rho_0 V_n\,\delta(F) \tag{59}$$

$$\frac{\partial(\rho v_i H)}{\partial t} + \frac{\partial}{\partial x_j}\left[(\rho v_i v_j + p\,\delta_{ij} + \sigma_{ij})\,H\right] = (p\,\delta_{ij} + \sigma_{ij})\,\nabla F\,\delta(F) \tag{60}$$

which is now valid in the entire space. Following Lighthill's methodology, we combine the time derivative of (59) with the divergence of (60) to form a wave propagation equation:

$$\frac{\partial^2(\rho' H)}{\partial t^2} - c_0^2\,\frac{\partial^2(\rho' H)}{\partial x_i^2} = \frac{\partial^2}{\partial x_i \partial x_j}(T_{ij} H) - \frac{\partial}{\partial x_i}\left[(p\,\delta_{ij} + \sigma_{ij})\,\nabla F\,\delta(F)\right] + \frac{\partial}{\partial t}(\rho_0 V_n\,\delta(F)) \tag{61}$$

with Lighthill's tensor defined in (42), and V_n is the wall normal velocity, positive when oriented outward the solid body.

The solution of (61) is obtained as previously using the free field Green's function:

$$\begin{aligned}\rho'(\mathbf{x},t) =& \frac{\partial^2}{\partial x_i \partial x_j} \int_{-\infty}^{t} \iiint_V \frac{\delta(t-\tau-|\mathbf{x}-\mathbf{y}|/c_0)}{4\pi c_0^2 |\mathbf{x}-\mathbf{y}|} T_{ij}(\mathbf{y},\tau)\,\mathrm{d}^3\mathbf{y}\,\mathrm{d}\tau \\ &- \frac{\partial}{\partial x_i} \int_{-\infty}^{t} \iint_{\partial V} \frac{\delta(t-\tau-|\mathbf{x}-\mathbf{y}|/c_0)}{4\pi c_0^2 |\mathbf{x}-\mathbf{y}|} \left[p\,\delta_{ij} + \sigma_{ij}\right](\mathbf{y},\tau)\, n_j\,\mathrm{d}^2\mathbf{y}\,\mathrm{d}\tau \\ &+ \frac{\partial}{\partial t} \int_{-\infty}^{t} \iint_{\partial V} \frac{\delta(t-\tau-|\mathbf{x}-\mathbf{y}|/c_0)}{4\pi c_0^2 |\mathbf{x}-\mathbf{y}|} \rho_0 V_n(\mathbf{y},\tau)\,\mathrm{d}^2\mathbf{y}\,\mathrm{d}\tau\,. \end{aligned} \tag{62}$$

The form (62) can be impractical for moving bodies, because the flow unsteadiness is preferably described in a frame of reference moving with the object. A better formulation involves the frame of reference $\boldsymbol{\eta}$ attached to the moving part. The retarded time is found by solving:

$$g(t^*,t,\mathbf{x},\boldsymbol{\eta}) \equiv t - t^* - \frac{|\mathbf{x}-\mathbf{y}(\boldsymbol{\eta},t^*)|}{c_0} = 0\,. \tag{63}$$

The power and elegance of the generalized function formulation becomes apparent when using the integration property of the Dirac function (Rienstra and Hirschberg, 2004):

$$\int_{-\infty}^{\infty} \delta\left(h(\xi)\right)\, f(\xi)\,\mathrm{d}\xi = \sum_i \frac{f(\xi_i)}{|h'(\xi_i)|}\,, \quad h(\xi_i) = 0 \tag{64}$$

which gives for the first integral of (62):

$$\int_{-\infty}^{t} \iiint_{V_\eta} \frac{\delta\left(g(\tau,t,\mathbf{x},\boldsymbol{\eta})\right)}{4\pi c_0^2 |\mathbf{x}-\mathbf{y}(\boldsymbol{\eta},\tau)|} T_{ij}\,\mathrm{d}^3\boldsymbol{\eta}\,\mathrm{d}\tau = \frac{1}{4\pi c_0^2} \iiint_{V_\eta} \left[\frac{T_{ij}}{R\,|1-\mathbf{M}.\mathbf{R}/R|}\right] \mathrm{d}^3\boldsymbol{\eta} \tag{65}$$

where the bracketed term is to be evaluated at the retarded time solution of (63) and at the corresponding position, $\mathbf{R} = \mathbf{x} - \mathbf{y}$, $\mathbf{M}$ is the vector Mach number of the sources expressed in the fixed frame of reference. The factor $1 - \mathbf{M}.\mathbf{R}/R$ is the Doppler factor of the sources, responsible for the frequency shift and convective amplification that occur when the source is moving with respect to the listener in a direction non-perpendicular to the line joining them. Ffowcs Williams and Hawkings analogy takes the form:

$$\begin{aligned}\rho'(\mathbf{x},t) =& \frac{1}{4\pi c_0^2} \frac{\partial^2}{\partial x_i \partial x_j} \iiint_{V_\eta} \left[\frac{T_{ij}}{R\,|1-\mathbf{M}.\mathbf{R}/R|}\right] \mathrm{d}^3\boldsymbol{\eta} \\ &- \frac{1}{4\pi c_0^2} \frac{\partial}{\partial x_i} \iint_{\partial V_\eta} \left[\frac{\left(p\,\delta_{ij} + \sigma_{ij}\right) n_j}{R\,|1-\mathbf{M}.\mathbf{R}/R|}\right] \mathrm{d}^2\boldsymbol{\eta} \\ &+ \frac{1}{4\pi c_0^2} \frac{\partial}{\partial t} \iint_{\partial V_\eta} \left[\frac{\rho_0 V_n}{R\,|1-\mathbf{M}.\mathbf{R}/R|}\right] \mathrm{d}^2\boldsymbol{\eta} \end{aligned} \tag{66}$$

The advantage of the formulation (66) over (62) is that it decouples the effects of flow unsteadiness, described in a frame reference attached to the body, from the ones related to the body motion. The proper use of the formulation (66) relies on the two following points (Roger, 2004):

- the flow intrinsic features (flow separation, turbulent transition, ...) are expressed in the frame of reference attached to the moving axes,

- the Doppler effects (convective amplification and frequency shift) are given by the motion of the sources in the fixed coordinate system.

The first and second integrals of (66) are, up to the Doppler factor, identical to those obtained in Curle's analogy, and correspond to the same physical mechanisms. For rotating machines, the dipolar integral is referred to as *loading noise*. The third integral of (66) is new, compared with Curle's previous result, and corresponds to the displacement of the fluid that is caused by the motion of the solid body. This source, called *thickness noise* in the context of rotating machines, is proportional to the volume of the solid body, and can thus be reduced by thinning the blades. It would normally only induce evanescent waves for subsonic speeds, but a time variation of the Doppler factor can induce a significant acoustic propagation, especially if the speed approaches the transonic regime.

One of the biggest achievements of the Ffowcs Williams and Hawkings formulation is the prediction of the noise produced by rotating machinery, accounting for the interfering modulations of the Doppler effects during the blades revolutions (Roger, 2004). But in order to proceed, we need first to estimate the order of magnitude of the different terms composing Eq. (66), to assess which simplifications are possible for the applications addressed in this course.

1.7.1 Dimensional Analysis and Source-Term Ranking

For propulsion systems based on propellers, it is customary to keep the tip Mach number safely below the transonic regime, in order to avoid large shock-associated aerodynamic penalties. In terms of noise ranking, it has been demonstrated (Goldstein, 1976) that in the subsonic regime, the ratio of acoustic powers related to the quadrupolar and loading noise sources scales as $W_q/W_d \sim M^2$, i.e. the quadrupolar contribution to the sound field can be effectively neglected. The same goes for the thickness noise, for Mach numbers up to roughly 0.7 (Glegg and Devenport, 2017).

The ranking between loading and thickness noise deserves further consideration. Due to the relative motion of the blade with respect to the listener, even a steady force will be generating noise, since the Doppler factor varies in time during the blade revolution. As a result, the *steady loading noise* can dominate the low-frequency tonal noise emitted by propellers immersed in reasonably uniform incoming flows, especially for mid-to-high subsonic Mach numbers and low blade counts. This is also the Mach regime for which the thickness noise can become significant, depending on the thickness of the blade tip. This complicates the ranking between the steady loading and thickness noise sources, the latter being strongly dependent on the blade tip geometry. But as soon as the flow field traversed by the blades becomes sufficiently distorted, typically through installation effects, the situation simplifies somehow, as the *unsteady loading noise* will usually take over and govern the sound field. The subsequent developments for rotating-blade noise rely so a large extent on this assumption, and will mostly address the loading noise sources.

2 Rotating-Blade Noise Formulations

2.1 Time-Domain Formulations

Once the formal solution of Ffowcs Williams & Hawkings' equation is obtained, the numerical implementation for practical use involves two steps. The first one is the determination of the source terms. Quadrupoles are not considered in subsonic rotating-blade noise studies. The monopoles in the expression of thickness noise are the explicit part of the formalism, since the kinematics of the blades is assumed prescribed. The dipole source strength of the loading-noise term is of more difficult access, because it is an information of unsteady aerodynamic nature, to be provided, for instance, by a dedicated CFD software. The second step is the calculation of the integrals, with efficient algorithms. The best practice for subsonic applications is provided by the formulation called 1A, developed by Farassat (2007) to *a priori* minimize discretization errors and computational time. Only retaining loading noise and thickness noise, it yields

$$4\pi\, p'_T(\mathbf{x},t) = \iint_{\partial V_\eta} \left[\frac{\rho_0\, \dot{V}_n}{R\,(1-M_r)^2} + \frac{\rho_0\, V_n\, \hat{R}_i\, \dot{M}_i}{R\,(1-M_r)^3} \right] \mathrm{d}^2\boldsymbol{\eta} + \iint_{\partial V_\eta} \left[\frac{\rho_0\, c_0\, V_n\, (M_r - M^2)}{R^2\,(1-M_r)^3} \right] \mathrm{d}^2\boldsymbol{\eta} \quad (67)$$

for the thickness noise, and

$$4\pi\, p'_L(\mathbf{x},t) = \iint_{\partial V_\eta} \left[\frac{\dot{p}\, \cos\theta}{c_0\, R\,(1-M_r)^2} + \frac{\hat{R}_i\, \dot{M}_i\, p\, \cos\theta}{c_0\, R\,(1-M_r)^3} \right] \mathrm{d}^2\boldsymbol{\eta} + \iint_{\partial V_\eta} \left[\frac{p\,(\cos\theta - M_i\, n_i)}{R^2\,(1-M_r)^2} + \frac{(M_r - M^2)\, p\, \cos\theta}{R^2\,(1-M_r)^3} \right] \mathrm{d}^2\boldsymbol{\eta} \quad (68)$$

for the loading noise. In those expressions, $M_r = \mathbf{M}.\mathbf{R}/R$ and $\hat{R}_i = \partial R/\partial x_i$.

Logically, the time-domain formulation is devoted in priority to impulsive noise sources, for which the time pressure signal features well-identified patterns of clear physical meaning (short-time blade-vortex interactions). For periodic signals, especially if the focus is put on a limited number of frequencies, the frequency-domain approach is preferred.

2.2 General Frequency-Domain Equations

2.2.1 The Rotating-Dipole Formula

Only the key steps of the derivations are given, details being beyond the scope of this document. Consider a compact blade element conventionally on the $\mathbf{e}_X$ axis at the origin of time, and its dipole strength, the reference frame and notations in Fig. 7. The expression of the radiated sound field reads

$$\tilde{p}^{(0)}(\mathbf{x},\omega) \;=\; \frac{1}{2\pi} \int_{-\infty}^{\infty} \frac{\mathrm{i}\, k\, R'_i\, F_i}{4\,\pi\, R'^2} \left\{ 1 \;-\; \frac{1}{\mathrm{i}\, k\, R'} \right\} \mathrm{e}^{\mathrm{i}\omega\,(t+R'/c_0)}\, \mathrm{d}t\,. \quad (69)$$

After expressing the scalar product $R'_i\,F_i$, introducing the Fourier transform $\tilde{F}(\omega)$ of the dipole strength $F(t)$, the expression of $\tilde{p}^0(\mathbf{x},\omega)$ becomes

$$\tilde{p}^{(0)}(\mathbf{x},\omega) \;=\; \frac{\mathrm{i}\,k\,R}{4\,\pi}\sum_{n=-\infty}^{\infty}\left\{\cos\gamma\,\cos\theta\,G_n^{(1)} \;+\; \sin\gamma\,\sin\theta\,G_n^{(2)}\right\}\,\tilde{F}(\omega-n\,\Omega)\,, \qquad (70)$$

with the auxiliary functions

$$G_j(t) \;=\; \sum_{n=-\infty}^{\infty} G_n^{(j)}\,\mathrm{e}^{-\mathrm{i}\,n\,2\,\pi t/T} \qquad G_n^{(j)} \;=\; \frac{1}{T}\int_{-T/2}^{T/2} G_j(t)\,\mathrm{e}^{\mathrm{i}\,n\,2\,\pi t/T}\,\mathrm{d}t\,,$$

$$G_1(t) \;=\; \frac{\mathrm{e}^{\mathrm{i}\,k\,R'}}{R'^2}\left(1-\frac{1}{\mathrm{i}\,k\,R'}\right)\,, \qquad G_2(t) \;=\; \sin(\Omega\,t-\phi)\,G_1(t)\,.$$

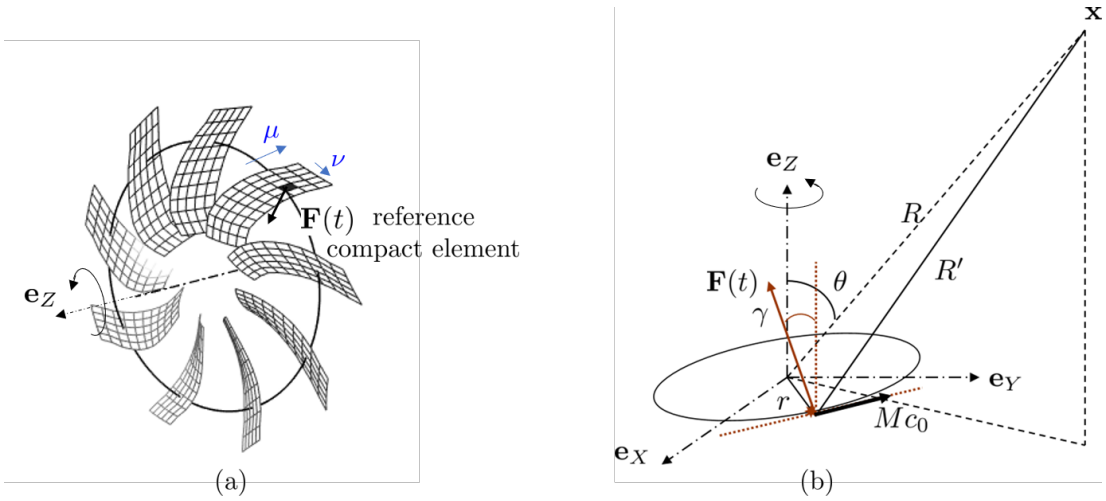


Figure 7: Rotor reference frame and main notations, for rotating-blade noise formulations. Surrounding fluid at rest.

Here R' stands for the exact distance of the element to the observer (see Fig.7-b). $\gamma(r)$ is the angle of the sectional dipole/force with respect to a parallel to the axis, or approximately the blade angle at radius r with respect to the rotational plane. The convention $\mathrm{e}^{-\mathrm{i}\,\omega t}$ is used for monochromatic waves. A single term of the sum defines a free-field radiation mode. Equation (70) features a fundamental property, which holds for any kind of force $\mathbf{F}(t)$: the acoustic pressure at point $\mathbf{x}$ and angular frequency ω is attributable to all components of the force at angular frequencies $\omega - n\,\Omega$, n being any relative integer. This property is the main effect of the frequency modulation induced by the constant-speed rotating motion.

In the acoustic and geometrical far field,

$$R'(t) \;\simeq\; R - r\,\sin\theta\,\cos(\Omega\,t-\phi) \qquad \frac{1}{R'^2} \;\simeq\; \frac{1}{R^2}\,,$$

so that the functions $G_j(t)$ are considerably simplified, as well as their Fourier series. The factors G_n^j are classically expressed in terms of Bessel functions. A closed-form expression

of the acoustic pressure is obtained, as

$$\tilde{p}^{(0)}(\mathbf{x},\omega) \;=\; \frac{\mathrm{i}k\,\mathrm{e}^{\mathrm{i}k\,R}}{4\pi\,R}\;\sum_{n=-\infty}^{\infty}\;(-\mathrm{i})^n\,\mathrm{J}_n\left(k\,r\,\sin\theta\right)\,\mathrm{e}^{\mathrm{i}\,n\,\phi}\;\left[\cos\gamma\,\cos\theta\;-\;\frac{n\,\sin\gamma}{k\,r}\right]\;\tilde{F}(\omega-n\,\Omega)\,. \tag{71}$$

2.2.2 Application to Rotor Tonal Noise

Tonal noise can only result from the periodicity of the force $F(t)$ with the period of rotation $2\pi/\Omega$. The origin of the periodic fluctuations is any azimuthal stationary distortion of the flow, as will be discussed later on. The force is expressed as the Fourier series

$$F(t) \;=\; \sum_{s=-\infty}^{\infty}\;F_s\,\mathrm{e}^{-\mathrm{i}\,s\,\Omega\,t}\qquad\qquad F_s\;=\;\frac{\Omega}{2\pi}\int_0^{2\pi/\Omega}\;F(t)\,\mathrm{e}^{\mathrm{i}\,s\,\Omega\,t}\,\mathrm{d}t\,,$$

leading to the expression of the source spectrum as a Dirac comb

$$\tilde{F}(\omega-n\,\Omega)\;=\;\sum_{s=-\infty}^{\infty}\;F_s\,\delta(\omega-(s+n)\Omega)\,.$$

As long as only a single blade element is considered, the sound field is also periodic with the period of rotation. For a rotor operating in a stationary distortion, the same element taken on all blades generates the same sound pressure, with a time delay. The Fourier transform of the total pressure signal is the sum of the Fourier transforms of the individual contributions. The latter are identical, except for a phase shift. The resulting sound of the array of B elements, if B denotes the number of blades, is the sound of the reference element multiplied by an interference function, which is simply the sum of all phase shifts. This sum is either equal to B if $N = mB$ is a multiple of B and zero otherwise. Finally, the tonal noise of a homogeneous rotor is emitted only at multiples of the blade passing frequency (BPF), as resulting from interference between blade contributions.

Introducing the wavenumber $k_{mB} = mB\,\Omega/c_0$, an expression for the sound pressure, valid everywhere in space, reads, for instance as found in Roger and Moreau (2008)

$$p_{mB}(\mathbf{x}) \;=\; \frac{\mathrm{i}\,k_{mB}r}{4\pi}\;\sum_{s=-\infty}^{\infty}\;F_s(r)\;\left\{\cos\theta\;\cos\gamma(r)\,\mathrm{G}^{(1)}_{mB-s}+\sin\theta\;\sin\gamma(r)\,\mathrm{G}^{(2)}_{mB-s}\right\}\,, \tag{72}$$

The factors $F_s(r)$ are the complex-valued coefficients of the Fourier series of the periodic force on the blade element acting as an equivalent rotating acoustic dipole. They are called blade-loading harmonics (BLH). The formula holds for the reference blade element of radius r, assumed acoustically compact and exactly on the axis $\mathbf{e}_X$ at the origin of time.

In the acoustic and geometric far field, Eq. (72) reduces to

$$p_{mB}(\mathbf{x}) \;=\; \frac{\mathrm{i}\,k_{mB}B\,\mathrm{e}^{\mathrm{i}\,k_{mB}\,R}}{4\pi\,R}\;\sum_{s=_\infty}^{\infty}\;\mathrm{e}^{\mathrm{i}\,(mB-s)(\phi-\pi/2)} \tag{73}$$

$$\times\;\left[\cos\theta\,F_s^A+\frac{(mB-s)\,F_s^T}{k_{mB}\,r}\right]\;\mathrm{J}_{mB-s}\left(k_{mB}\,r\sin\theta\right)\;,$$

$F_s^A = F_s \cos\gamma$ and $F_s^T = F_s \sin\gamma$ being the axial and tangential blade force components. For axial-flow architectures, the radial force on blade elements is most often negligible, except for blades with significant sweep. A more complete and general expression including a radial force component is given in section 2.2.4.

2.2.3 General Discretized Formulation

Assuming that the thickness is much smaller than the acoustics wavelengths of interest, the blades can be reduced to their mean-camber surfaces and the local unsteady lift considered as dipole source term. This reduction is typically considered in analytical formulations, but it still requires that the geometry and the aerodynamics are known, prior to any sound prediction. In cases where this information is unknown, approximations can be obtained with simplified methods, assimilating blade segments to flat plates, for mathematical tractability (see the lecture *Semi-analytical and low-order models applied to isolated and installed propulsors*).

Meshing the mean-camber surface is simply achieved by numbering the compact cells of the mesh with two indices μ and ν in the radial/spanwise and chordwise directions, respectively, from some mid-surface cell chosen as reference. The total sound formulation is obtained from Eq. (73) by adding a double sum over indices μ and ν, provided that a proper phase is given each cell to account for its position at the origin of time. The expression of $\mathbf{F}\cdot\mathbf{R}'$ for an arbitrary element becomes

$$\mathbf{F}\cdot\mathbf{R}' \;=\; FR\left\{\cos\gamma\,\left(\cos\theta - \frac{z_{\mu\nu}}{R}\right) \;+\; \sin\gamma\,\sin\theta\,\sin(\Omega t - \phi + \phi_{\mu\nu})\right\}\,,$$

if $\phi_{\mu\nu}$ and $z_{\mu\nu}$ denote the angular and vertical positioning offsets of the element at the origin of time with respect to the reference element. The derivations are extended in a straightforward way.

The factors $\phi_{\mu\nu}$ and $z_{\mu\nu}$ generate relative phase-shifts between the mesh cells, essential for the structuration of the interference between all contributions to the sound. They account for the main blade-design parameters, such as chord, stagger, camber, twist and so on. Because propagation-path differences remain at any observation distance, they also have an effect in the far-field approximation. Indeed, for the cell of indices (μ,ν) at some reference radius R_0,

$$R' \;\simeq\; R - z_{\mu,\nu}\,\cos\theta - R_0\,\sin\theta\,\cos(\phi - \phi_{\mu,\nu} - \Omega t)\,.$$

In the acoustic and geometric far field, Eq. (72) reduces to

$$p_{mB}(\mathbf{x}) \;=\; \frac{\mathrm{i}\,k_{mB}B\,\mathrm{e}^{\mathrm{i}\,k_{mB}\,R}}{4\pi\,R}\sum_{\mu,\nu}\sum_{s=\infty}^{\infty}\mathrm{e}^{\mathrm{i}\,(mB-s)(\phi-\phi_{\mu\nu}-\pi/2)}\,\mathrm{e}^{-\mathrm{i}\,k_{mB}\,z_{\mu\nu}\cos\theta}$$
$$\times\left[\cos\theta\,F^A_{s,\mu\nu} + \frac{(mB-s)\,F^T_{s,\mu\nu}}{k_{mB}\,r_\mu}\right]\,\mathrm{J}_{mB-s}\left(k_{mB}\,r_\mu\sin\theta\right)\,. \qquad (74)$$

This equation and Eq. (73) are the most currently used background for tonal noise predictions, except in direct numerical simulation strategies. It must be kept in mind that, in the general case of cambered blades, the force angle γ also depends on (μ,ν). Therefore, the axial and tangential force components $F^A_{s,\mu\nu} = F_{s,\mu\nu}\cos\gamma_{\mu,\nu}$ and $F^T_{s,\mu\nu} = -F_{s,\mu\nu}\sin\gamma_{\mu,\nu}$ are better expressed as such.

2.2.4 Effect of Axial Forward Flight

Previous formulae were presented for a rotor or propeller at rest, assuming a homogeneous propagation medium also at rest. For a propeller in flight, the effect of the relative motion with respect to the medium needs to be included, so that convective amplification effects are also reproduced. The problem is best formulated in a reference frame attached to the propeller, considering a stationary observer in this frame and a fluid in uniform motion. This reproduces what would be the conditions of wind-tunnel testing, and suppresses the Doppler effect that would be perceived during the fly-over of an aircraft. This effect can always be reconstructed if needed. But the involved propeller-noise mechanisms are better analyzed in stationary conditions. The generalization of Eq. (74) is given below for a flight speed of Mach number $M_a = U_a/c_0$ perfectly aligned with the rotational axis, fluid motion being in the negative Z direction, same as for the induced speed. A more general expression, considering a non-zero incidence of the propeller, was given by Hanson and Parzych (1993). For completeness, a radial force, often ignored in axial-flow architectures, is also included.

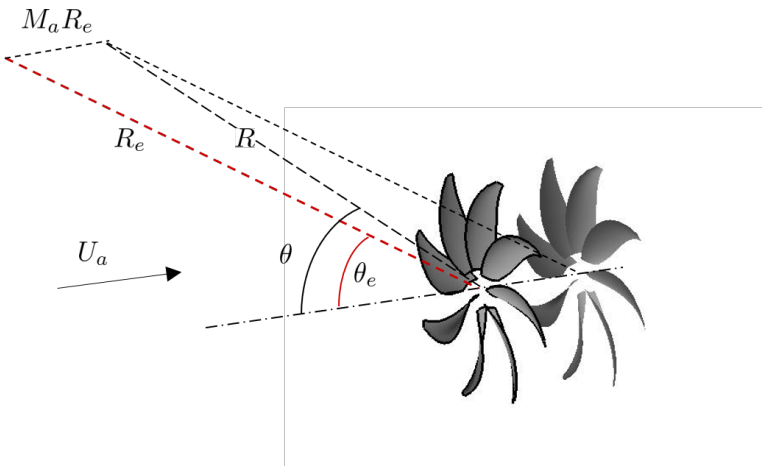


Figure 8: Notations for the problem statement of a propeller in forward flight, showing the emission coordinates of the center point (R_e, θ_e).

The formula reads

$$p_{mB}(\mathbf{x}) = \frac{\mathrm{i}\, k_{mB} B\, \mathrm{e}^{\mathrm{i}\, k_{mB}\, R_e}}{4\pi\, R_e\, (1 - M_a \cos\theta_e)} \sum_{\mu,\nu} \sum_{s=\infty}^{\infty} \mathrm{e}^{\mathrm{i}\,(mB-s)(\phi-\phi_{\mu\nu}-\pi/2)}\, \mathrm{e}^{-\mathrm{i}\, k_{mB}\, z_{\mu\nu} \cos\theta_e/(1-M_a\cos\theta_e)}$$
$$\times \left\{ \left[\frac{\cos\theta_e\, F^A_{s,\mu\nu}}{1 - M_a\cos\theta_e} + \frac{(mB-s)\, F^T_{s,\mu\nu}}{k_{mB}\, r_\mu} \right] \mathrm{J}_{mB-s}\left(\frac{k_{mB}\, R_\mu \sin\theta_e}{1 - M_a\cos\theta_e} \right) \right. \tag{75}$$
$$\left. + \mathrm{i}\, \frac{\sin\theta_e\, F^R_{s,\mu\nu}}{1 - M_a\cos\theta_e}\, \mathrm{J}'_{mB-s}\left(\frac{k_{mB}\, R_\mu \sin\theta_e}{1 - M_a\cos\theta_e} \right) \right\}$$

with the notations

$$R_e = \frac{1}{\beta_a^2}\, (S_0 + M_a\, R \cos\theta)\ , \qquad S_0 = R\, \sqrt{1 - M_a^2 \sin^2\theta}$$

and $\beta_a = \sqrt{1 - M_a^2}$ with $M_a = U_a/c_0$. θ_e is the angle defined in Fig. 8. Here μ and ν again stand for the element indices in the spanwise and chordwise directions of a blade mesh. $z_{\mu\nu}$ is the axial coordinate of the element of indices (μ, ν) along the direction of the axial flow and $\phi_{\mu\nu}$ the angular offset of the element at the origin of time.

2.3 Loading-Noise Mechanisms

A physical interpretation of Eq. (73) and of its subsequent developments (74)-(75) can be elaborated considering Figure 9, illustrating a case with $B = 4$. It can be first observed that source data at several rotational frequencies $s\Omega$ (the Blade Loading Harmonics, BLHs) contribute to the acoustic field at a single rotational frequency $mB\Omega$ (the Blade Passing Frequency Harmonic, BPFH). This translates the Doppler frequency shift resulting from the relative motion of the blade with respect to the steady listener, which is continuously and periodically modulated during one revolution.

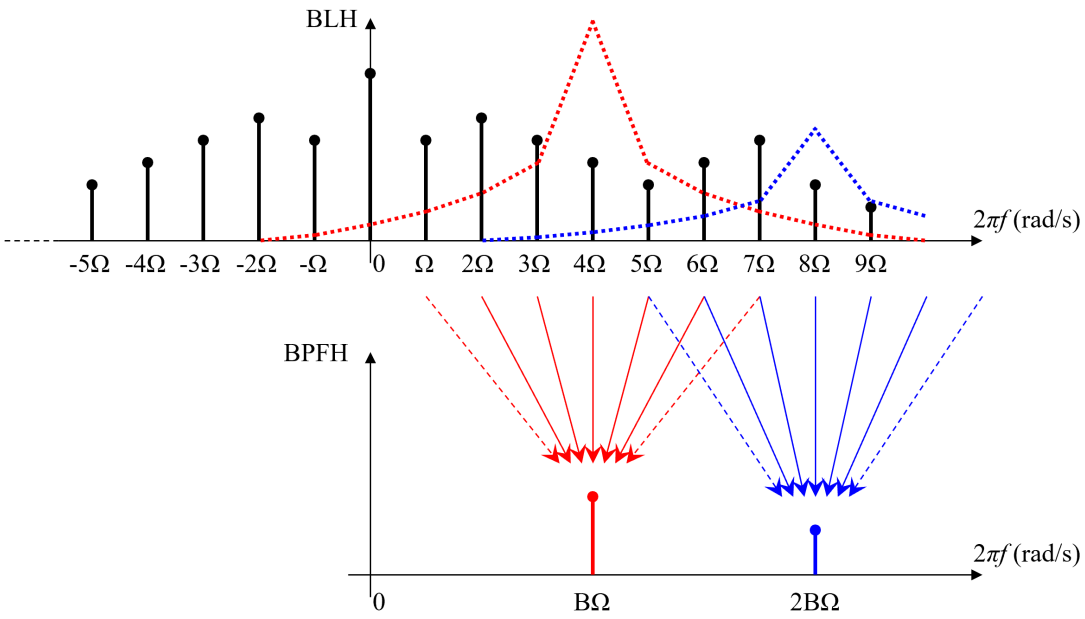


Figure 9: Graphical interpretation of the Blade Loading Harmonics summation of Eq. (73) involved in the calculation of the tonal sound field at each Blade Passing Frequency Harmonic m.

If the summation in (73) involves theoretically an infinite number of BLHs, in practice the contribution of each BLH of order s is dictated by the amplitude of the Bessel function $\mathrm{J}_{mB-s}(k_{mB}\, r\, \sin\theta)$. The argument of this function can be expressed as a tangential Mach number: $k_{mB}\, r = mB\,\Omega\, r/c_0$, i.e. is generally small for subsonic propellers and low BPFH orders. Figure 10 shows that for low values of its argument, the Bessel function of first kind and order 0 (i.e. $s = mB$) has the largest amplitude, followed by the first few integer orders.

In other words, for low tangential Mach numbers of the blades, and for low BPFH orders m, and/or for low polar angles θ of the listener, the sound field is dominated by the BLHs with frequencies that aren't too far from the considered BPFH. A B-bladed



Figure 10: Bessel function of first kind and integer order.

propeller will radiate more noise if it traverses a flow distortion having an azimuthal periodicity of order B as well.

As a corollary, for the blades steady-loading to be significant, the ingested flow has to be quite homogeneous, the tangential Mach number not too small, and the propeller should not contain too many blades. Those conditions are typically encountered in small drone applications, for which the first couple of BPFHs can be strongly linked to the steady-loading, hence mean propeller thrust. For these applications, reducing the dominant tonal noise without compromising the propulsive thrust can be challenging (Sarikaya et al., 2024).

References

Batchelor, G. K. (1967). *An Introduction to Fluid Dynamics*. Cambridge University Press, Cambridge.

Colonius, T. and Lele, S. K. (2004). Computational aeroacoustics: progress on nonlinear problems of sound generation. *Progress in Aerospace Sciences*, 40:345–416.

Crighton, D. G., Dowling, A. P., Williams, J. E. F., Heckl, M., and Leppington, F. G. (1992). *Modern Methods in Analytical Acoustics — Lecture Notes*. Springer-Verlag London.

Curle, N. (1955). The influence of solid boundaries upon aerodynamic sound. *Proceeding of the Royal Society of London*, A231:505–514.

Dowling, A. and Williams, J. E. F. (1983). *Sound and sources of sound*. Ellis Horwood-Publishers.

Farassat, F. (2007). Derivation of formulations 1 and 1a of farassat. Technical Report TM-2007-214853, NASA.

Glegg, S. and Devenport, W. (2017). *Aeroacoustics of low Mach number flows: fundamentals, analysis, and measurement*. Academic Press.

Goldstein, M. E. (1976). *Aeroacoustics*. McGraw-Hill International Book Company.

Hanson, D. and Parzych, D. (1993). Theory for noise of propellers in angular inflow with parametric studies and experimental validation. Technical report, NASA CR 4499.

Ianniello, S. (2007). New perspectives in the use of the ffowcs williams–hawkings equation for aeroacoustic analysis of rotating blades. *Journal of Fluid Mechanics*, 570:79–127.

Lighthill, M. J. (1952). On sound generated aerodynamically. Part I. General theory. *Proceeding of the Royal Society of London*, A211:564–587.

Lighthill, M. J. (1954). On sound generated aerodynamically. Part II. Turbulence as a source of sound. *Proceeding of the Royal Society of London*, A222:1–32.

Pérot, F., Auger, J. M., Giardi, H., Bailly, C., and Juvé, D. (2004). Computation of the noise generated by low Mach number flows around a cylinder and a wall-mounted half-cylinder. In *10th AIAA/CEAS Aeroacoustics Conference*, number 2004-2859, Manchester, UK.

Powell, A. (1960). Aerodynamic noise and the plane boundary. *Journal of the Acoustical Society of America*, 32(8):982–990.

Rienstra, S. W. and Hirschberg, A. (2004). *An Introduction to Acoustics*. Eindhoven University of Technology.

Roger, M. (2004). Noise from moving surfaces. In *Advances in aeroacoustics and applications*. von Karman Institute, Rhode-St-Genèse.

Roger, M. and Moreau, S. (2008). Aero-acoustic installation effects in cooling fan systems, part i: scattering by surrounding surfaces. In *ISROMAC-12*, Paper 2008-20222, Honolulu HA.

Sarikaya, B., Zarri, A., Christophe, J., Aissa, M. H., Verstraete, T., and Schram, C. (2024). Aerodynamic and aeroacoustic design optimization of uavs using a surrogate model. *Journal of Sound and Vibration*, page 118539.

Wang, M. and Moin, P. (2000). Computation of trailing edge flow and noise using large-eddy simulation. *AIAA Journal*, 38(12):2201–2209.

Williams, J. E. F. and Hawkings, D. L. (1969). Sound generated by turbulence and surfaces in arbitrary motion. *Philosophical Transactions of the Royal Society of London, Series A: Mathematical and Physical Sciences*, 264(1151):321–342.